heritage

MDPI

Article

Climate Change and Cultural Heritage: From Small- to Large-Scale Effects—The Case Study of Nora (Sardinia, Italy)

Fabio Sitzia [1,2]

[1] HERCULES Laboratory, Institute for Advanced Studies and Research, University of Évora, Largo Marquês de Marialva 8, 7000-809 Évora, Portugal; fsitzia@uevora.pt
[2] Geosciences Department, School of Sciences and Technology, University of Évora, Rua Romão Ramalho 59, 7000-671 Évora, Portugal

Abstract: Rising sea levels are mainly due to increases in environmental temperatures that are causing ice to melt. The weathering of geomaterials is mainly due to the increase in the concentration of greenhouse gases in the atmosphere. This research addresses current and future sea level rises and their weathering effects on the building stones in the Phoenician–Punic archaeological area of Nora (Sardinia, Italy). Some forecasting models, selected according to real-world scenarios (shared socioeconomic pathways—SSPs), give a definitive overview of both the rising sea levels and stone weathering conditions in Nora. The year 2100 A.D. was selected as the base of our investigations because the SSPs are scenarios of projected socioeconomic global changes up to 2100 A.D. The data on the expected alteration of geomaterials were reconstructed by considering the temperatures, the rainfall amount, and the atmospheric CO_2 of every scenario. This was made possible by knowing the current degree of alteration of the geomaterials and their weathering resistance. The rising sea level models were obtained through the SSPs scenarios data and built using geographic information systems software. The projections show a slowing down of the weathering degrees of the stone materials in Nora. This is due to the increase in the average annual temperature and the decrease in the average annual rainfall. However, it is shown that some other factors, such as the marine spray in the area, could accelerate the decay. Projections of the rising sea levels show how the settlement will be partially submerged, losing between 3.54% and 8.49% of the emerged land. The models provided a maximum ingression of the coastline, ranging from 23.7 m to 29.5 m, based on the severity of the scenarios. Coastline-shifting maps indicate the flooding of some buildings located on the western coast of Nora, the most sensitive part of the territory.

Keywords: geoarchaeology; sea level rise; climate change; cultural heritage; ancient mining activity; shared socioeconomic pathways (SSPs)

Citation: Sitzia, F. Climate Change and Cultural Heritage: From Small- to Large-Scale Effects—The Case Study of Nora (Sardinia, Italy). *Heritage* **2022**, *5*, 3495–3514. https://doi.org/10.3390/heritage5040181

Academic Editors: Humberto Varum, Vasilis Sarhosis and Fernanda Prestileo

Received: 8 October 2022
Accepted: 11 November 2022
Published: 17 November 2022

1. Introduction

With global warming, there has been an increase in the average temperature of Earth, starting from 9th century A.D. and carrying on until present day. This is mainly due to the intensification of greenhouse gas emissions (CO_2, CH_4, and N_2O) and is associated with the escalation of extreme atmospheric phenomena (flooding, desertification, and drought), which result in environmental, social, economic, sanitary, and cultural changes [1]. Recent studies have addressed a large number of UNESCO heritage sites from all over the world that are threatened by climate change [2].

Some of the most evident and alarming outcomes of climate change on coastal cultural heritage buildings can be easily grouped according to their scale:

(i) On a small scale, we can observe the weathering of geomaterials caused by rainwater acidification and dry pollution depositions [3,4].
(ii) On a large scale, we can observe the rising sea levels [5].

Those topics are discussed in this work through a consideration of a case study—the coastal archaeological area of Nora, situated in southwest Sardinia, Italy (Figure 1).

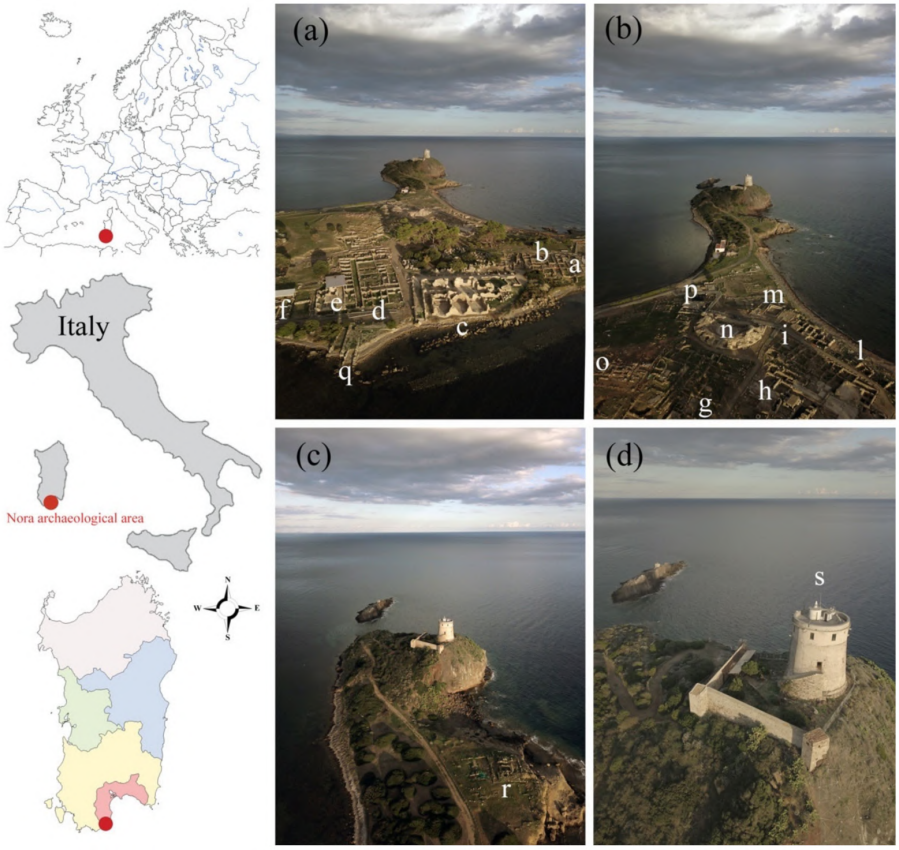

Figure 1. (**a**–**d**) The archaeological area of Nora: geographical location (Europe, Italy, Sardinia) and main buildings. a—tetrastyle atrium house; b—*Tronchetti* director house; c—sea spa; d—polyfunctional complex; e—little spa; f—shophouse complex; g—kasbah; h—*ninfeo*; i—late-antique houses of the central district; l—coastal houses; m—*fullonica*; n—great theatre; o—*Tanit* temple; p—Roman *forum*; q—Christian basilica; r—sacred area; s—*Coltellazzo* tower.

Here, the stone building materials are presently being subjected to weathering that is believed to be different from that which they will be subjected to in the future, due to climate change.

The coastline ingression in Nora, due to the rising sea, is submerging some of the ancient city buildings and is increasing coastal erosion. This is the reason that several studies have already focused on this issue in the different locations of the Mediterranean Sea [2,5] and in Africa [6].

Built near a preexisting Nuragic site, later Punic and Roman, and located on the Capo Pula headland, Nora is one of the most important archaeological sites in Italy.

From a geographical–physical point of view, this headland originated from an ancient volcanic island which, in recent times, has joined the mainland via a sandy isthmus.

In Nora, signs of Nuragic presence were found, attesting to the inhabitance of the site during the Bronze Age [7]. Traces of the Nuragic–Phoenician repopulation date back to the 8th cent. B.C., while the oldest remains are a necropolis with tombs, dated to the end of 7th and the beginning of the 6th cent. B.C. [8].

During the Roman conquest of Sardinia (238 B.C.), Nora was probably the most important city on the island together with *Tharros* [9]. The remains currently present in Nora testify to the development of the city during the 2nd and 3rd cent. A.D. Numerous buildings of the ancient Roman city are preserved, such as the *forum*, theatre, amphitheater (not yet excavated), thermal houses, and residential houses.

The locals started to abandon Nora mainly because they gradually withdrew to safer places in the inner parts of the island [7].

The first excavation in the Nora archaeological area dates back to the end of the 19th century. A systematic survey was carried out between 1952 and 1960 by Gennaro Pesce [7].

The oldest archaeological surveys in Nora date back to 1967 at the ancient port [10]. This landing place was used for the mooring of freight ships from Spain, Greece, the Italian peninsula, Southern Gaul, and Africa. Today, the remains of the port are submerged under water owing to the sea level, which must have been between -1.4 and −1.6 m lower during the Roman period, as is discussed later in this paper.

From the investigations of Di Gregorio et al. [11], the variation in the sea levels in Nora since the Roman era was also ascertained from some historical quarries. A section of the quarries, located near the coast—in order to facilitate the transport of materials by sea—are presently underwater. In the extractive area of the northeastern cove, the quarry foot is presently between −0.30 m and −0.56 m a.s.l. [12]. It can be deduced that the quarrying area was originally wider towards the east, between 4 and 7 m beyond the current coastline. Recent archaeological research on Nora has focused on the creation of digital renderings of the buildings, 3D digital models, and virtual tours, to increase the usability of the archaeological site [13,14]. These geospatial technologies and remote sensing applications are often used and play important roles, such as the identification and evaluation of the potential risks affecting the archaeological areas [15,16].

In particular, digital processing can be useful for monitoring the archaeological site against coastal erosion, due to the rise in sea levels that is expected to continue in the coming decades [17].

Apart from the sea levels rising, climate change also has small-scale consequences, through the weathering of the building materials of the archaeological area. It has been ascertained that Nora was built using four main local lithotypes.

Recently, the durability of rhyodacite and the Tyrrhenian sandstone of Nora have been evaluated by accelerated ageing tests in controlled environments [18,19].

Most of the decay of the building materials in Nora is due to the high humidity and saline atmosphere. In order to mitigate the corrosion of the stone, due to saline water in the theater, a coating was applied in 1979. However, the use of this coating has only accelerated the decaying process [20,21].

In this paper, the actual and the future decay of the building materials in Nora are examined. Models of the rising sea levels in the promontory, provided for the year 2100 A.D. according to the shared socioeconomic pathway scenarios, are developed. The work aims to present a strategic climate change risk assessment to raise awareness among the authorities, in the hope that they will develop an ordinary maintenance plan for the site that can include the application of protective coatings on the stone. On a larger scale, this maintenance could involve technological solutions in order to control the rising of the sea, such as floodgates. This work has been carried out in the aim of avoiding the need for future research and archaeological fieldwork being conducted underwater.

2. Mining Activity and Extracted Materials in Nora

Three quarters of the archaeological area is built on outcrops of the lower basic intermediate lava sequence (LBLS) belonging to the first Oligo–Miocene volcanic cycle that occurred in Sardinia [22,23]. The northern area has been developed on marine and continental sediments of the Quaternary age [24]. Located to the Northwest, about 5 km from the archaeological area, the reliefs of the mountain belt of *Sarroch-Pula-Domus De Maria* are characterized by large leucogranite outcrops and granodiorites dating back to the Upper Carboniferous (Figure 2) [25].

Figure 2. Geological map with the indication of the main ancient quarries and mines in the area of Nora.

The Nora peninsula is separated from these reliefs by a piedmont strip with an average slope of 15%, consisting of ancient continental deposits from the Pleistocene age together with siltstone and sandstone of the *Cixerri* formation (Eocene–Oligocene) [24].

The supply of stone for building purposes in Nora is known from the Roman period [26]. In particular, the stone made its appearance in Nora buildings as early as the Late Punic period [7], representing classical examples of vernacular architecture [27].

The archaeological area has been built by the use of granites, rhyodacites, *Cixerri*, and Thyrrenian sandstones extracted from nearby quarries (Figure 2).

No ancient granite quarries have been identified. This lithology, mainly used as ashlars, often features in rounded and shapeless building elements, suggesting the sampling of erratic boulders from high-energy environments (beaches or riverbeds).

The main ancient quarry of rhyodacites has been identified at *Monte Su Casteddu* [28], (coordinates 39°0′48.90″ N; 8°59′49.47″ E). The materials extracted here were probably transported by water along the Rio Pula to the ancient port [29]. Other traces of mining activity on rhyodacites outcrops are located at *S. Vittoria–Guventeddu*, *S. Efisio*, and *Agumu* (Figure 2).

Sa Perdera (coordinates 39°1′26.54″ N; 8°57′34.15″ E, Figure 2), located to the northwest of Nora, is considered to be the ancient quarry of *Cixerri* sandstone [30]. Some chronological considerations revealed that the lithotype was used in buildings dating back to 6th cent. B.C.; this testifies to an early exploitation of quarries, as well as confirming the use of sandstone to produce stalks. This quarry, active during the Roman period, was exploited in contemporary times for the construction of the bridge over the Pula River and the Church of San Giovanni Battista (14th cent. A.D.), both located in Pula. In Nora, sandstones from the *Cixerri* formation were used for ashlars and the production of artifacts.

The main quarry of Thyrrenian sandstones can be found west of the site of Nora at *Fradis Minoris* (coordinates 38°59′7.96″ N; 9°0′14.23″ E, Figure 2). This quarry extends over an area of about 12,000 m^2, with approximately 5000 m^3 of extracted materials, and is currently not active [31]. The Thyrrenian sandstone used for the construction of the archaeological site was utilized for a multitude of archaeological elements, from ashlar to column shafts.

The surrounding outcrops of Nora were exploited for ancient and contemporary mining activities which focus on the extraction of metals. Ancient mines are already documented in the locality of *Perdu Carta* (Figure 2) in 18th cent. D.C. Here, the extraction of silver galena (Ag-PbS) occurred. According to historical archaeological reconstructions, *Perdu Carta* was already active during the Roman and Phoenician–Punic period [32]. In contemporary times, it is known that, in 1881, in the locality of *Sa Galanza* (4 km northwest of Nora), the exploration of silver galena was active; meanwhile, in the nearby localities of *Monte Santo* and *Padenteddu*, ferrous minerals were extracted [33]. The mining activities in the foothills of *Sarroch-Pula-Domus De Maria* began in Roman times and would have persisted until the early 1960s.

It remains unclear where the limestone quarries for mortar production were located because no calcareous outcrops are present in the area. The raw calcareous material could have been extracted from the nearby Roman city *Karalis* (present-day *Cagliari*), located 37 km to the northeast.

Limestones also surface at *Monte Lapanu* (32 km to the west) in the *facies* of the meta-calcareous and dolomitic formation of *Gonnesa* (Lower Cambrian) [34]. Here, information about the mining activity during the Roman period has been known since the 1980s [35]. At *Monte Lapanu*, extractions are also documented in contemporary times up to the abandonment of the quarries, which occurred after the bankruptcy of the mining company. The ancient quarries have been incorporated within the *Teulada* military range since 1956.

In Figure 2, above the quarry/mine symbols, we have written the respective location names. Below the symbols, information about the extracted material is exhibited. Pb—lead; Ag—silver; Rhy—rhyodacites; Thy—Thyrrenian sandstones; CxS—*Cixerri* sandstones.

3. Petrographic and Physical Characterization of Nora Stone Building Materials

In Thyrrenian sandstones, a microsparitic carbonate cement binds well-rounded clasts of quartz, feldspar, biotite, pyroxene, and olivine (Figure 3a). The stone consists of rich fossil fauna (e.g., coelenterates, algae, bivalves, and gastropods).

The rhyodacites (Figure 3b), seen under an optical microscope, present a porphyritic structure and hyalopilitic texture. Paragenesis consists of phenocrysts of plagioclase, clinopyroxene, hornblende, and magnetite.

Under optical microscopy, Nora granites (Figure 3c) display the characteristics of equigranular leucogranites (syenogranites) with microgranitic and porphyric facies. Paragenesis consists of K-feldspar, quartz, rare plagioclase, and biotite.

In *Cixerri* sandstones, quartz, biotite, and muscovite crystals are bound by carbonatic cement (Figure 3d).

Table 1 shows the physical characteristics of the materials just described.

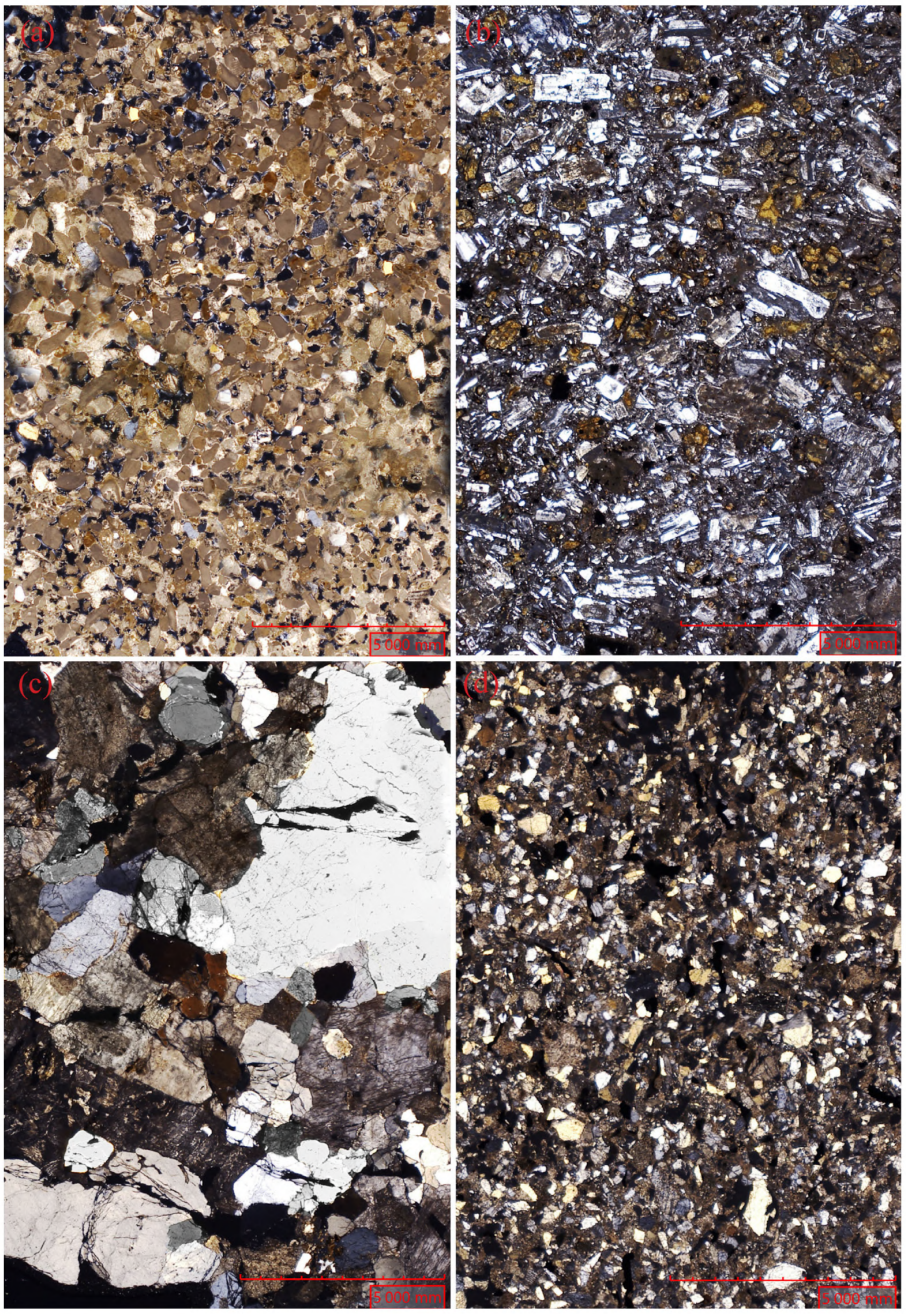

Figure 3. Building materials from the ancient city of Nora: (**a**) Thyrrenian sandstone; (**b**) rhyodacite; (**c**) granite; (**d**) *Cixerri* sandstone.

Table 1. Physical–mechanical average features of building materials from the Nora settlement. The number of samples tested for the calculation of the physical properties is indicated in square brackets.

Physical–Mechanical Properties	**Stone Building Materials in Nora Site**			
	Granite	**Rhyodacite**	**Thyrrenian Sandstone**	***Cixerri* Sandstone**
Bulk density (ρ_B, g/cm^3) [5]	2.61 ± 0.04	1.65 ± 0.06	1.65 ± 0.08	1.84 ± 0.05
Efficacy porosity (Φ_O, %) [5]	7 ± 3.9	23 ± 1.9	38 ± 3.8	29 ± 1.6
Closed porosity (Φ_C, %) [5]	1.7 ± 0.9	2.1 ± 0.9	3.8 ± 0.5	4.5 ± 0.4

Table 1. *Cont.*

Physical–Mechanical Properties	Stone Building Materials in Nora Site			
	Granite	**Rhyodacite**	**Thyrrenian Sandstone**	***Cixerri* Sandstone**
Saturation index (*S.I.*, %) [5]	88 ± 7.2	94 ± 6.4	86 ± 3.7	81 ± 5
Total immersion coefficient (CI_W, %) [5]	3 ± 1.7	11 ± 6.4	20 ± 2.9	7 ± 3.1
Weight lost on immersion (W_{DC}, g/g) [5]	0.0047 ± 0.015	0	0.022 ± 0.01	0.01 ± 0.002
Point load strength index (Is_{50}, MPa) [5]	1.64 ± 0.2	7 ± 2.9	0.7 ± 0.3	0.5 ± 0.3
Compressive strength (σ_C, MPa) [5]	23 ± 2.6	143 ± 58.3	10 ± 4.1	7 ± 4.7
Thermal conductivity (k, W/m·K) [3]	2.99 ± 0.28	1.09 ± 0.10	1.21 ± 0.32	1.43 ± 0.15
Volume heat capacity (s, J/m^3·K) [3]	$1.31\times 10^6 \pm 3.3 \times 10^4$	$1.88 \times 10^6 \pm 4.7 \times 10^4$	$1.66 \times 10^6 \pm 2.7 \times 10^4$	$1.55 \times 10^6 \pm 3.9 \times 10^4$
Thermal diffusivity (α, m^2/s) [3]	$2.27 \times 10^{-6} \pm 2.25 \times 10^{-8}$	$0.59 \times 10^{-6} \pm 4.84 \times 10^{-8}$	$0.72 \times 10^{-6} \pm 1.54 \times 10^{-7}$	$0.92 \times 10^{-6} \pm 7.25 \times 10^{-8}$
Leeb D hardness (L_H, HLD) [6]	570 ± 97	675 ± 18	445 ± 68	350 ± 29
Vapor permeability (k_V, g/m·s·Pa) [1]	1.5×10^{-11}	2.6×10^{-11}	3.5×10^{-11}	1.8×10^{-11}
Gas driven permeability (k_G, mDarcy) [6]	5.4 ± 5	N/A	3350 ± 1000	43 ± 22
P wave speed (V_P, m/s) [3]	2410 ± 71	3906 ± 71	2326 ± 117	1905 ± 81
S wave speed (V_S, m/s) [3]	1268 ± 56	1914 ± 31	1192 ± 20	1075 ± 11

4. Materials and Methods

About 2 kg of Thyrrenian sandstone, rhyodacite, granite, and *Cixerri* sandstone were collected in the ancient quarries and have been cut to specifications following the normative test. The wet mass (m_W) of the samples was determined after 10 days of immersion.

The bulk volume V_B was calculated as:

$$V_B = ((m_W - m_{HY})/\rho_{W25^\circ C})100$$

where m_{HY} is the hydrostatic mass of the wet specimen and $\rho_{W25\,^\circ C}$ is the water density (0.9970 g/cm^3) at a temperature of 25 °C. Helium open porosity (ΦHe) and closed porosity (Φ_C) were calculated as:

$$\Phi He = ((V_B - V_R)/V_B)100$$

$$\Phi_C = ((V_R - V_S)/V_S)100$$

where V_R and V_S, respectively, represent the real and solid fraction volume of the samples, both measured by a Quantachrome ULTRAPY1200e Pycnometer (Figure 4a).

The bulk density (ρ_B, g/cm^3) was calculated as:

$$\rho_B = m_D/V_B$$

Total immersion coefficient (C_{IW}) and saturation index (*S.I.*) were computed as:

$$C_{IW} = ((m_W - m_D)/m_D)100$$

$$S.I. = (\Phi H_2O/\Phi He)100$$

Hardness was measured by a portable tester—Leeb D EQUOTIP (Proceq)—with the wireless software platform EQUOTIP LIVE version 3.1.1 (Figure 4b). The instrument was indirectly verified, according to the ISO16859-2 normative.

Figure 4. (**a**) Quantachrome ULTRAPY1200e Pycnometer; (**b**) Leeb D EQUOTIP; (**c**) permeameter TINY PERM 3; (**d**) PUNDIT PL200 PROCEQ; (**e**) Thermal Effusively Meter ISOMET; (**f**) special containers for vapor permeability; (**g**) Point Load Tester mod. Controls D550 Instrument.

The gas-driven permeability was measured by a handheld air permeameter—TINY PERM 3—with NER-supplied android wireless storing data software (Figure 4c).

Measurements of the P and S waves speeds (*Vp*, *Vs*) were carried out using a portable PUNDIT PL200 PROCEQ (Figure 4d).

The thermal conductivity coefficient was measured by a Thermal Effusively Meter ISOMET 2114 equipped with a surface probe (range 0.3–3.0 W/mK) (Figure 4e).

For the water vapor permeability test, the normative UNI EN 15803/2010 was followed. Specimens were previously dried in the oven for 24 h at 60 ± 5 °C to eliminate the humidity until a constant mass was reached. Each one of the dried specimens was weighed to obtain the dry mass (m_d).

Special containers (Figure 4f) were prepared to receive the stone specimens. To create an entirely moisture-saturated environment, cotton wool with 1 cm of distilled water was placed in each container. Afterwards, each stone specimen was placed on the opening of the container and all the possible air gaps were sealed with silicone mastic. For each set, the container, the water, and the stone specimen were weighed (m_i) and then placed inside an ARALAB FITOCLIMA 300 EDTU climate chamber. This chamber was programmed to maintain 20 °C and 40% of relative humidity as required by the normative ASTM E96/E96M-16 (Standard Test Methods for Water Vapor Transmission of Materials).

Sets were weighed continuously each 24 h after the beginning of the test. The end of test was reached when the sets achieved a mass difference equal to 0.1%.

Water vapor flux, G_w, was estimated from the average of the differences between mass by time unit (in g/h) of at least three values obtained in steady-state flow. Water vapor permeability, W_{VP}, is given in kg/m·s·Pa through the following equation:

$$W_{VP} = (G_W \cdot h)/(A_S \cdot \Delta P \cdot 36 \times 10^5)$$

where G_W—water vapor flux (g/h); h—specimen thickness (m); A_S—specimens tested area (m^2); ΔP—pressure difference of water vapor inside and outside the container (Pa).

The point load index (Is_{50}) was determined with a point load tester (mod. Controls D550 Instrument, Figure 4g). The compressive strength (σ_C) was indirectly calculated according to [36].

Optical microscope (OM) observations were acquired with an optic Leica DM2500M microscope (Leica Microsystems, Wetzlar, Germany) in polarized NX light. Thin sections of 30 µm thickness were analyzed according to normative UNI EN 12407:2019.

The mineralogical composition of the stones were identified by X-ray diffraction with a Bruker D8 Discover diffractometer (Bruker Company, AXS Karlsruhe, Germany) with CuKα radiation tube operating at 40 kV and 40 mA. The XRD peaks were measured between 2° and 75° 2θ, with 1 s counting time per point. The Powder Diffraction Database (PDF-ICDD, International Centre for Diffraction Data) using the Bruker EVA software was used to identify the crystalline phase.

In order to build the flood models planned for 2100 A.D., a GIS procedure using QGIS 3.20 ODENSE was employed. A digital elevation model (DEM), based on a 2008 LIDAR flight, was obtained at a 1 m resolution from the Sardegna Geoportale https://www.sardegnageoportale.it (accessed on 30 April 2022).

Sea level rise values for 2100 A.D. were selected according to the average value of five shared socioeconomic pathways (SSPs) using the IPCC Sixth Assessment Report on climate change [37]. The used values were as follows: SSP1-1.9 = +38 cm; SSP1-2.6 = +44 cm; SSP2-4.5 = +56 cm; SSP3-7.0 = +68 cm; SSP5-8.5 = +77 cm.

In the DEM, possibly due to a margin of error in the original data, the coastline corresponded to the 50 cm level, which was taken as the baseline for the analysis [5].

The areas below 50 cm were extracted from the DEM raster and transformed into polygons to illustrate the current sea level. The same was performed for +38, +44, +56, +68, and +77 cm, corresponding to each of the models.

5. Results and Discussion

The Effects of Climate Change on Building Materials

The response of stones to weathering is mainly linked to the amount of annual rainfall and the temperature. In Nora, in the period 1971–2000, the average annual rainfall was recorded to be 395 mm and the average annual temperature was 17.7 °C. These data came from the nearest meteorological station of *Elmas*, located about 30 km to the northeast.

In these climatic conditions, building stone materials suffer from moderate chemical weathering [38]. This is caused by the water reacting with the paragenesis mineral in rocks to form clays, minerals, and soluble salts. These reactions occur especially when the water is slightly acidic. The responses of stone building materials under weathering depends on the chemical composition and some physical–mechanical features (Table 1).

The granite in Nora mainly exhibits a physical alteration of "arenization" (Figure 5b). In granite ashlars, the alteration begins with rainwater penetrating through the discontinuity framework between crystals. Rainwater has the capability to reach quite deep levels, causing or, in any case accelerating, the alteration processes. Developments occur on the basis of physical and chemical mechanisms. Among the factors that regulate the physical-mechanical decay there are (i) thermoclastism; (ii) the penetration of meteoric waters; (iii) the formation of crystals of soluble substances, especially in marine environments.

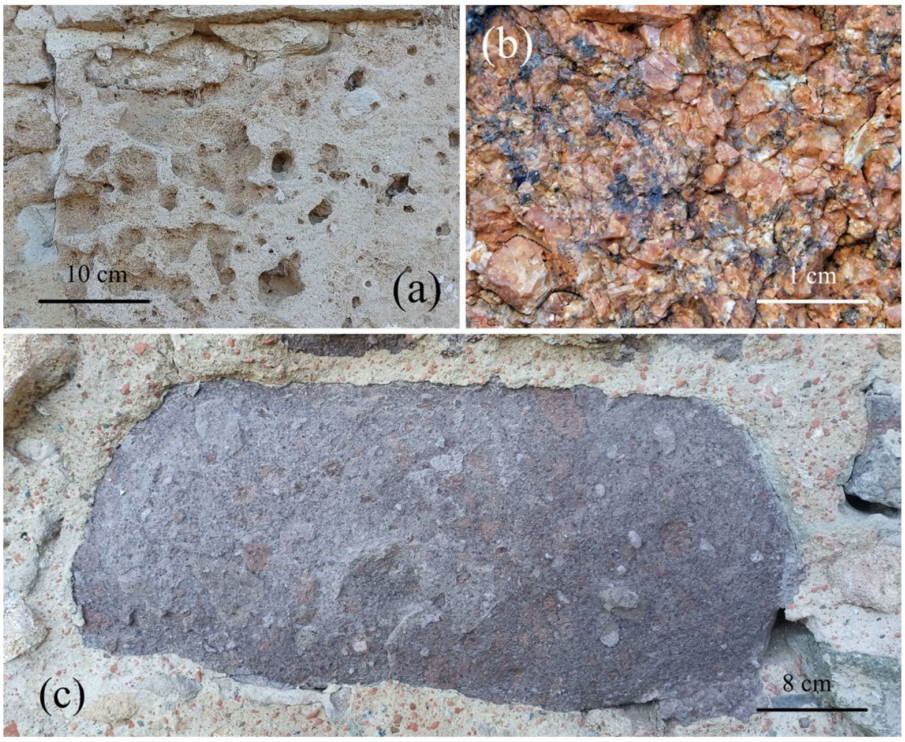

Figure 5. Stone materials alterations: (**a**) alveolisation of the Thyrrenian sandstone; (**b**) arenization of the leucogranite; (**c**) exfoliation and physical decohesion of the rhyodacite.

In the area of Nora, the effect of freezing–thawing is negligible because of an average of 4 days per year with temperatures less than 0 °C.

The granite arenization led to the formation of saprolites, an arenaceous regolith consisting of different chemical compositions according to the local climate. In Mediterranean saprolites, kaolin minerals such as gibbsite can reach 40–80% in the <2 μm fraction [39]. In Nora, the decohesion products of granite consist of gravel and sandy–gravel clastic materials often used as aggregate in the ancient mortars [40].

Granites are subjected to carbo-hydrolysis [41,42], a chemical weathering of the K-feldspar and plagioclase altered in neoformed kaolinite (detected in XRD diffraction, Table 2). This type of alteration is typical of humid and warm climates. The reaction involved in the carbo-hydrolysis is as follows:

$$2KAlSi_3O_8 \text{ (K-feldspar)} + 2H^+ + 9H_2O \rightarrow Al_2Si_2O_5(OH)_4 \text{ (Kaolinite)} + 2K^+ + 4SiO_2 + 8H_2O \quad (1)$$

$$2NaAlSi_3O_8 \text{ (Albite)} + 11H_2O + 2CO_2 \rightarrow Al_2Si_2O_5(OH)_4 \text{ (Kaolinite)} + 2Na^+ + 2HCO^- + 4H_4SiO_4 \quad (2)$$

Thyrrenian sandstone in Nora suffers both physical and chemical alterations.

It also suffers from exfoliation, alveolisation (Figure 5a) and granular decohesion "arenization" with 0.5% gravel, 74.9% sand, and 24.7% silt/clay residue. Granular decohesion is responsible for the loss of shape of the worked stone and its artistic detail. This is caused by the sulfation process of the carbonate cement of the stone according to the common following reaction:

$$CaCO_3 + SO_2 + 0.5O_2 \rightarrow CaSO_4 + CO_2 \quad (3)$$

Thyrrenian sandstones are imbibed by rainwater and marine spray due to their high effective porosity (38%) and permeability of about 3 Darcy (Table 1). When the calcium carbonate (water solubility of 0.014 g/l at 293 K) is converted into gypsum (water solubility of 2.6 g/l at 293 K), the cement framework of the stone loses its bounding capacity. The outcome is granular decohesion, which results in a decrease in the stone's mechanical strength. The gypsum in Thyrrenian sandstones was detected by XRD (Table 2). The

sulphation processes in Nora, as previously illustrated, are due to the marine atmosphere; however, sulphation can also originate from anthropic emissions in urban areas.

Table 2. pXRD for Nora stone materials: Ca—calcite; Qz—quartz; Pla—plagioclase; Kf—K-feldspar; Bio—biotite; Gy—gypsum; Kao—kaolinite; Mu—muscovite; Zeo—zeolite; Ver—vermiculite; Tr—traces (≤2% wt.); "•" indicates present (2–10% wt.); "••" indicates abundant (10–40% wt.); "•••" indicates very abundant (≥40% wt.)

Stone Materials	Ca	Qz	Pla	Kf	Bio	Gy	Kao	Mu	Zeo	Ver
Leucogranite	-	•••	••	•	Tr	-	Tr	-	-	-
Thyrrenian sandstone	•••	••	•	-	-	Tr	-	Tr	-	-
Cixerri Sandstone	••	•••	•	••	•	-	-	-	-	Tr
Rhyodacite	-	•	•••	-	-	Tr	-	-	•	-

Cixerri sandstone suffers from exfoliation and granular decohesion that occurs due to the same physical–chemical principle that moderates the Thyrrenian sandstones.

Rhyodacites have an autoclastic brecciated structure with a chaotic presence of lava clasts with diameters from 1 to 30 cm, which are immersed in a glassier lava matrix, with a basically dacitic composition and characterized by a lower degree of welding with respect to the same clasts. This type of structure favors a differential alteration in the rock essentially due to the different physical–mechanical characteristics of the glass matrix and the clasts. In fact, these have a higher mechanical strength than the glass matrix; so, under the action of atmospheric decay, there is an enucleation of the same clasts. The rhyodacites also are affected by exfoliation, as shown in Figure 5c. In rhyodacites, the chemical alteration is highlighted by the presence of zeolites (Table 2).

The current decay dynamics of building stones in Nora could be modified according to the forecasted environmental conditions caused by climate change.

According to the simulations of the Climate Change Knowledge Portal (multi-model ensemble), Sardinia will be subjected to changes in average annual temperature and rainfall in 2100 A.D. These are defined on the basis of shared socioeconomic pathways (SSPs) scenarios that take into account the greenhouse gas emissions for 2100 A.D. [43,44]. These scenarios have been formulated to help develop the IPCC Sixth Assessment Report on climate change, published in August 2021. IPCC consists of five progressively serious scenarios (SSP1-1.9, SSP1-2.6, SSP2-4.5, SSP3-7.0, and SSP5-8.5), which account for CO_2 air concentrations in 2100 A.D. which are 380, 430, 550, 860, and 1020 ppm respectively. The present-day CO_2 air concentration is 410 ppm.

SSP1-1.9, also called "sustainability", is considered to be the most optimistic scenario, whereby an increase in average annual temperature of +0.93 °C and +41 mm increase in average annual rainfall will occur.

SSP1-2.6 is again an optimistic scenario, indicating that Sardinia will be affected by an anomaly temperature increase of +1.28 °C and a decrease in average rainfall of −25 mm.

In the "Regional Rivalry" SSP2-4.5 scenario, an increase in average annual temperature of 2.16 °C and a decrease in average rainfall of −39 mm, in comparison with the present-day values, are expected.

In the SSP3-7.0 scenario, an increase in average annual temperature of 3.22 °C and a decrease in average rainfall of −64 mm, in comparison with the present-day values, are expected. The last and extreme scenario (SSP5-8.5) indicates a temperature increase of 4.3 °C and a rainfall decrease of −93 mm in Sardinia.

The data of the provided climatic conditions (T and rainfall amount) of the five 2100 A.D. scenarios were arranged in a Peltier diagram [38] (Figure 6). The plot shows that, for SSP1-1.9 and SPP1-2.6, moderate chemical weathering on the stone is presumed, similar to the current one. The SSP2-4.5, SSP3-7.0, and SSP5-8.5 scenarios are all characterized

by an increase in average temperature and decrease in average rainfall; the stone will be subjected to very slight weathering.

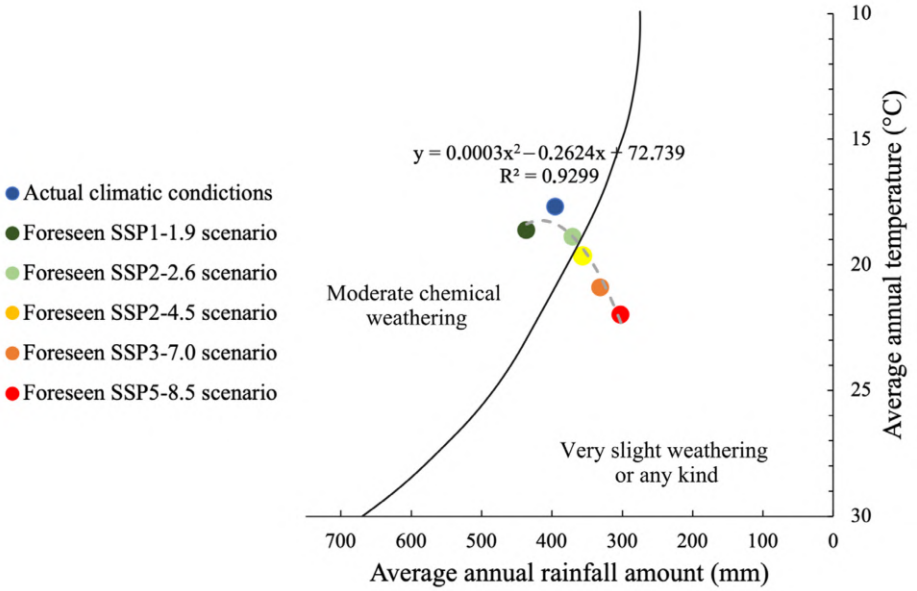

Figure 6. Changes in weathering dynamics according to present-day climatic conditions and foreseen SSPs scenarios.

Regarding the physical decay of the stones, environmental warming will reduce the freezing–thawing processes in Nora. They are already extremely rare (4 days per year) and will be decreased by −0.26 days for the most likely scenario, SSP2-4.5, and by −0.27 for both SSP3-7.0 and SSP5-8.5.

Increases in temperature and decreases in relative humidity and rainfall could break the frequency of the solubilization/crystallization cycles of the salt phases in the stone.

Recent ongoing studies are also evaluating the dynamics of stone biodegradation based on future climatic conditions.

Although the two aforementioned variables, T and rH, indicated a decrease in weathering, the problem is actually extremely complex. Particularly for carbonate cement stone, another three factors contribute to carbonate weathering [45].

(i) Rainwater acidification due to CO_2 atmospheric increase (karst effect) according to [4]:

$$CaCO_3 + CO_2 + H_2O = Ca(HCO_3)_2 \quad (4)$$

(ii) Additional rainwater acidification due to atmospheric sulfuric (H_2SO_4) and nitric acids (HNO_3).

(iii) Dry deposition of pollutants SO_2 and NO_X.

All three contributions are computed into the Lipfert equation, giving a value of surface recession rate expressed in μm/m, calculated for 330 ppm of atmospheric CO_2 concentration at 20 °C [46]. Lipfert equations for the baseline period 1961–1999 indicated a surface regression in Europe between ~25 and ~5 μm/year. The value is higher in Northern and Central Europe due to the high value of average annual rainfall.

The contribution of Karst effects in the Lipfert equations is higher and is supposed to stay more or less constant in the far future. The effects given by additional rainwater acidification due to atmospheric sulfuric (H_2SO_4) and nitric acids (HNO_3) and dry deposition of pollutant SO_2 and NO_X is supposed to decrease [45]. Europe will experience an alkalinization of rainwater due to the decrease in SO_X and NO_X air concentrations [47].

The SSPs scenarios confirm that SO_2 emissions in 2100 A.D. will decrease from the current ~100 Mt/yr to ~10 Mt/yr for the SSP1-1.9 scenario and to ~80 Mt/yr for the SSP5-8.5 scenario.

Additionally, SSP1-1.9 and SSP1-2.6 indicate that NO_2 emissions in 2100 A.D. will decrease from the current ~10.8 Mt/yr to ~8.2 Mt/yr. Contrarily, an increase to 8.4, 12.6, and 20.5 Mt/yr for SSP2-4.5, SSP5-8.5, and SSP3-7.0, respectively, is provided.

A correction of the Lipfert equations was performed by modifying the parameter pCO_2 at 800 ppm with a temperature of 25 °C. These corrections are suggested by the A2 emission scenarios for the far future (2070–2099) [48].

This concentration is similar to the one expected for the SSP3-7.0 scenario for 2100 A.D.

The corrected data indicate an increase in surface regression in Europe of up to 30 µm/year. The higher increase will happen in Northern and Central Europe and no/negative changes are expected starting form a baseline data in Southern Europe (period 1961–1999) [45]. For Sardinia, a decrease in surface regression of up to −1 µm/year is provided for the period 2070–2099.

In the Nora area, weathering is amplified by the presence of marine spray, which the Lipfert equation does not account for. The peninsula is in fact affected by an average monthly concentration of marine aerosols ($3.26 \times 10^{-8} < M_{Spray} < 3.61 \times 10^{-8}$ kg/m^3; data from GIOVANNI software; https://giovanni.gsfc.nasa.gov/giovanni), with high deposition rates due to winds with an average annual speed of 15.3 km/h.

On silicatic rocks, for example on granites, the process of carbo-hydrolysis could increase due to a higher concentration of CO_2 (chemical reaction [1]).

The stones in Nora will probably react to the climate change features in different ways, because many atmospheric weathering parameters can individually or contemporarily act by favoring or containing the decay.

6. The Outcomes of Climate Change on the Archaeological Area

The area of the Nora Peninsula represents an ecosystem in balance with a high degree of sensitivity.

Due to the action of wave motion, it is subject to coastal erosion and geomorphological instability. The action of wave motion is intense in conjunction with winds from the southern quadrants.

Various sources elaborate on the serious consequences of coastal erosion on the archaeological area. In particular, the coastline in correspondence to the coastal houses (building l in Figure 1), is subjected to an elevated degree of susceptibility to retreat. The same problem affects an 80 m-long coastline portion immediately to the north of the Christian Basilica. A modest regression characterizes the northwestern coast of the peninsula. The remaining stretches of coast have a stable degree of susceptibility to retreat. Some other areas, such as a stretch of coast south of the Christian Basilica, have a tendency to advance instead [49].

Historically, the Nora coastline and the coastal lagoons have undergone radical modifications following fluctuations in sea levels. Past sea levels have been documented, for example, by analyzing the coastal quarries. At *San't Efisio*, the surveys carried out for the Noramar project [12] highlighted that the quarry foot is today submerged at −0.30 m and −0.56 m a.s.l.; a sea level variation of approximately +1.40–+1.60 m, between the Roman age and the present day, can be assumed [50]. Data and cores reveal how the nearby lagoon of Nora was an emerged area during the Roman period. Furthermore, the morphology of the seabed in front of the *Fradis Minoris* quarry means that, in ancient times, the emerged surface of the peninsula was wider, with a coastline shifted up to 50 m.

The Nora district will be affected by the rising sea levels, linked to climatic change, in the future.

The rise in sea levels is linked to eustasy, glacio-hydro-isostasy, tectonics, and local parameters, such as soil compaction [51]. In Figures 7 and 8, the maps of the coastline position scenarios provided for 2100 A.D. are shown.

The present-day extension of the archaeological area shown in Figure 7a, selected as the zone with a higher concentration of ancient buildings, is about 7.61 hectares. In Table 3, a report on sea level changes, coastline shifts, and submerged areas for each scenario is provided.

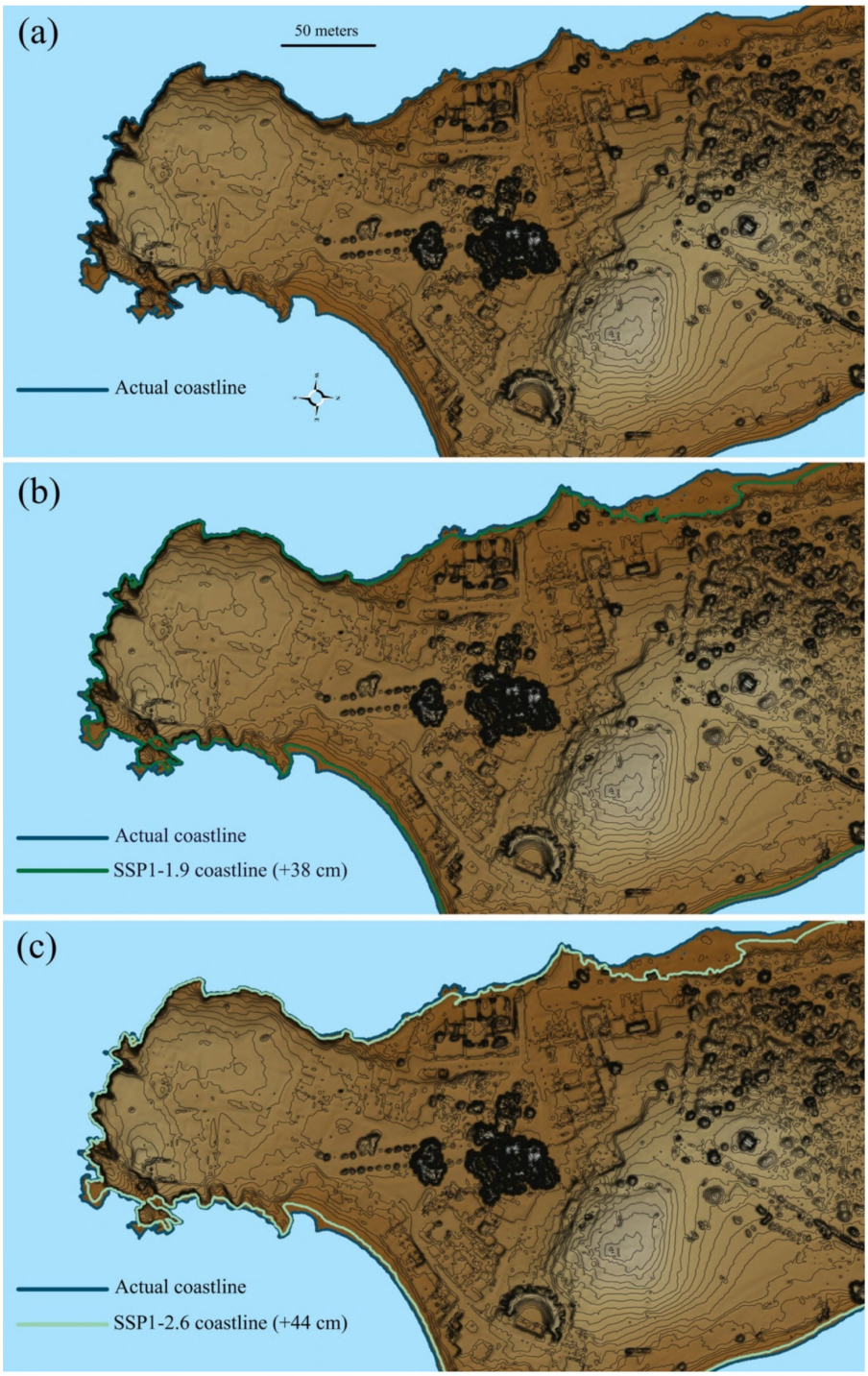

Figure 7. Flooding models for Nora archaeological area provided in year 2100 A.D.: (**a**) present-day coastline position; (**b**) SSP1-1.9 scenario (+38 cm); (**c**) SSP1-2.6 scenario (+44 cm).

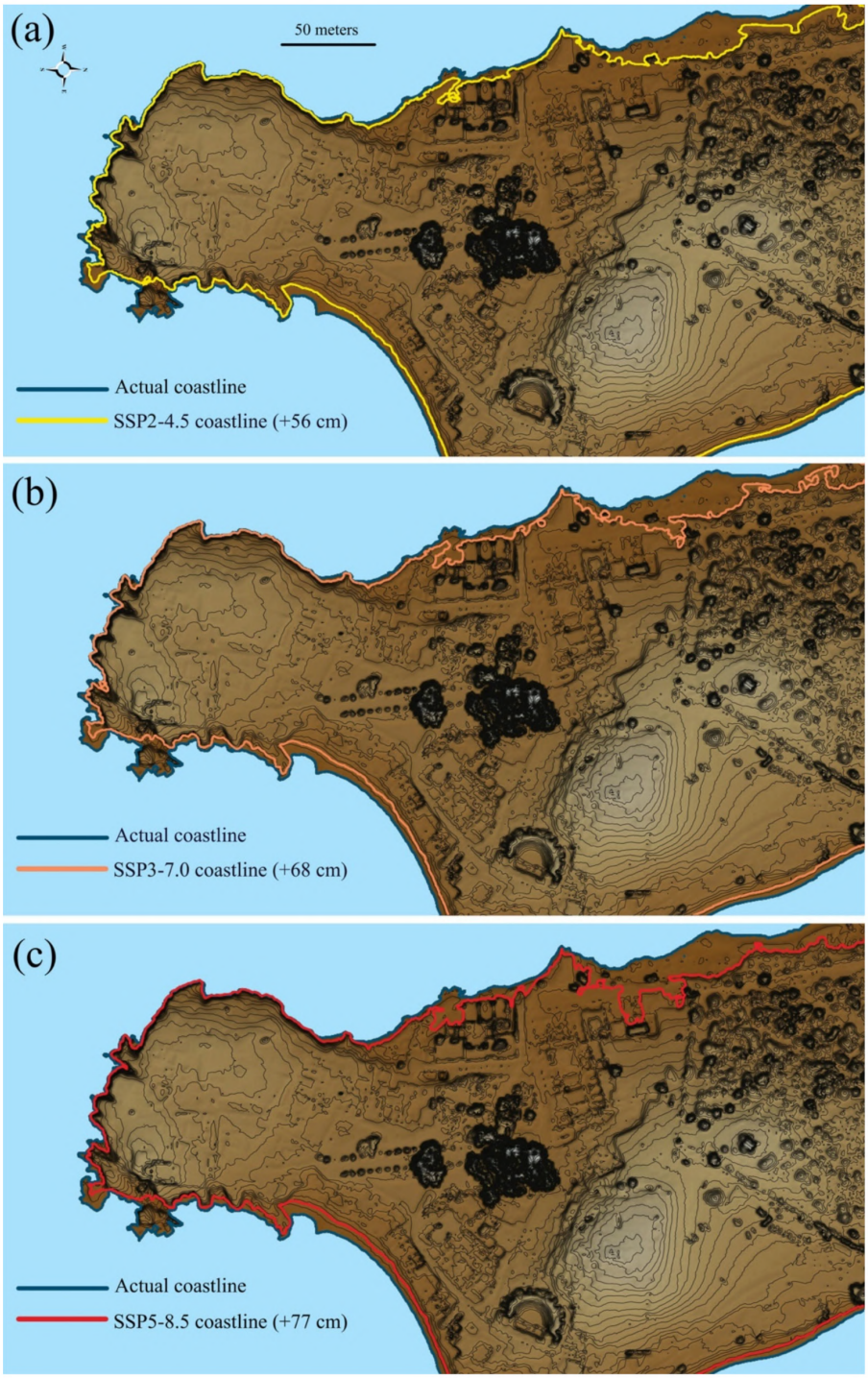

Figure 8. Flooding models for Nora archaeological area provided in year 2100 A.D.: (**a**) SSP2-4.5 scenario (+56 cm); (**b**) SSP3-7.0 scenario (+68 cm); (**c**) SSP5-8.5 scenario (+77 cm).

Table 3. Sea level change and coastline shifting provided for 2100 A.D. in Nora. The submerged area and the percentage of submerged area are calculated according to the current site extension represented on Figures 7 and 8 (7.61 hectares).

Year 2100 A.D. Scenario	Average Sea Level Change (cm)	Coastline Shifting Max (m)	Submerged Area (Hectares)	Submerged Surface (%)
SSP1-1.9	38	23.7	7.34	3.54
SSP1-2.6	44	23.9	7.2	5.39
SSP2-4.5	56	24.1	7.13	6.35
SSP3-7.0	68	26.2	7.01	7.92
SSP5-8.5	77	28.5	6.95	8.69

In Figure 7b, the coastline provided by the scenario SSP1-1.9 is represented. In this case, the coastline shifting (S) in the various areas of the archaeological site is calculated as max 23.7 m. With this scenario, a portion of 3.54% of the present-day extension will be submerged, reducing the surface from 7.61 hectares to 7.34 hectares.

Under SSP1-2.6, the coastline shifting is calculated as 23.9 m, which is very similar to the previous scenario (Table 3, Figure 7c).

In the most probable scenario for 2100 A.D., SSP2-4.5, the scenario indicates a reduction of 6.35% of the present-day emerged surface. In Figure 8a, it is shown that the Christian Basilica remains (building Q in Figure 1) but will be further submerged.

In the most serious scenarios, SSP3-7.0 and SSP5-8.5, the portion of the Nora peninsula under examination would reduce to 7.01 and 6.95 hectares, respectively. It would therefore lose 7.92 and 8.69% of the current extension, respectively (Table 3, Figure 8b,c). The coastline would stretch inland up to 26.2 and 28.5 m, respectively, compared with the current position.

In the SSP3-7.0 scenario, a partial flooding of the large baths is noted (Figure 8b).

In the most pessimistic scenario, the +77 cm rise will cause flooding in the small spas (building E in Figure 1) and in the shophouse complex (building F in Figure 1). In the southern sector, the new coastline will lap the coastal houses in this scenario. The current coastline position and the one in SSP5-8.5 have been plotted on the orthophotos of the large baths (Figure 9a) and coastal houses (Figure 9b).

As is evident in Figures 8 and 9, the west coast of Nora is the most affected by sea level rise. Here, an artificial breakwater has already been installed near the large thermal baths.

The coastline in this position would allow the waves to directly reach the local structures, causing extensive damage to the buildings. It would also increase the process of coastal erosion, to the detriment of the buildings themselves.

Note that these models do not account for the rising of the sea that is caused by the astronomical tides (around 10 cm) or the meteorological tides. The latter are due to the wind coming from the southern quadrants, that are present throughout the year, but that reach a maximum speed and frequency in the periods of September–October and March–April.

Not only, the rise in sea levels is linked to land vertical movements, isostatic rates and local parameters, such as soil compaction that were not taken into account in this text.

Additionally, the sea level changes represented in our model are only an average of a calculated range between the maximum and the minimum. For example, the projection of SSP5-8.5 indicates a range between 55 and 124 cm, where +77 cm, shown in this paper, is the average value. It is clear that the maximum value of +124 cm could completely flood some buildings.

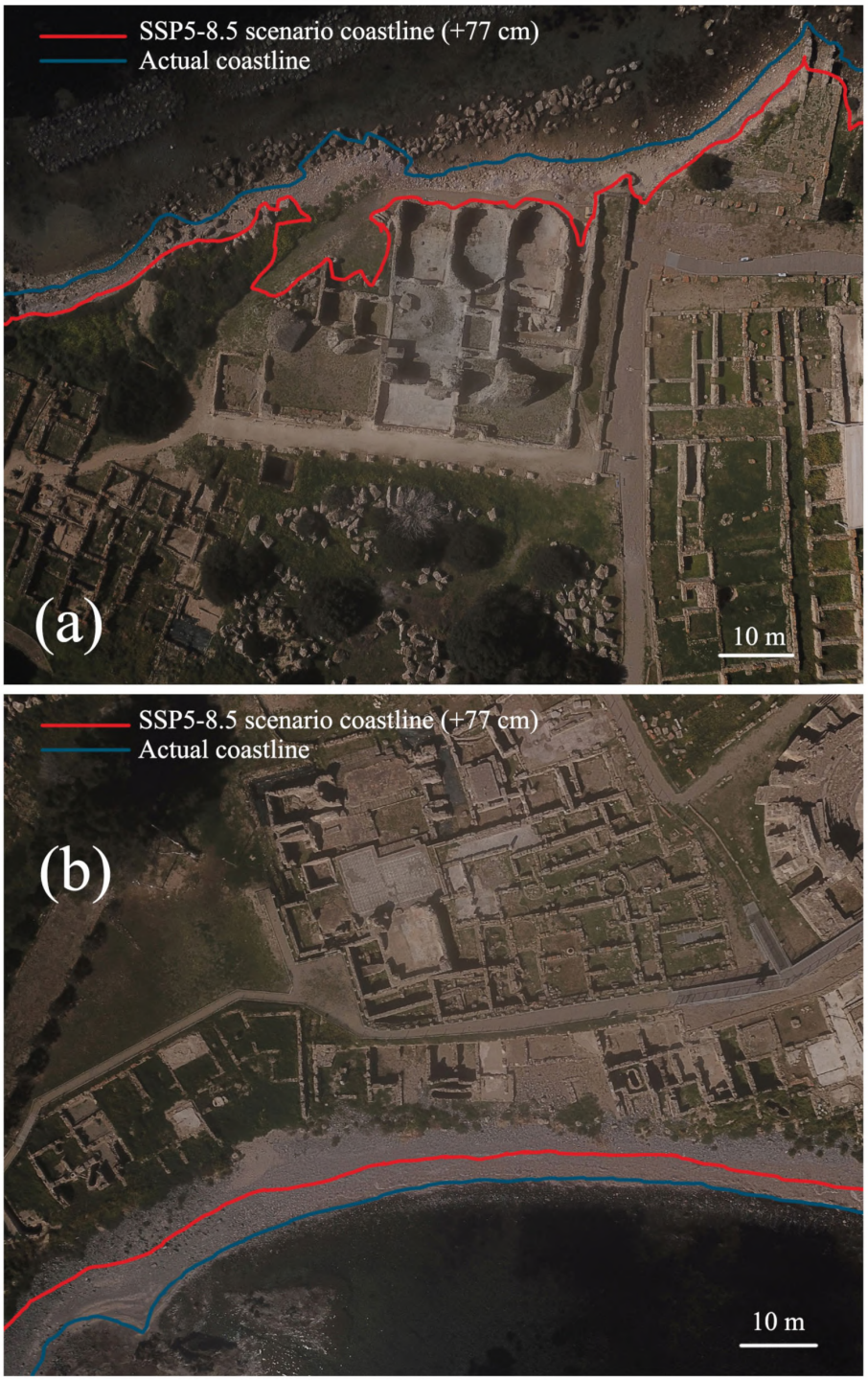

Figure 9. Archaeological area of Nora: (**a**) present-day and SSP5-8.6-predicted coastline on sea spa; (**b**) present-day and SSP5-8.6-predicted coastline on coastal houses.

7. Conclusions

This study has archaeological superintendencies and local authorities as stakeholders, and provides a valid tool for understanding how climate change could cause definitive damage in the Nora archaeological area.

Regarding the behavior of stone materials in the future, some hypotheses have been performed. Understanding whether the decay will decrease or increase is a rather complicated challenge. This is because a high amount of marine spray in Nora complicates the decay projections.

However, climate simulations using accelerated decay tests (ageing) which are currently in progress will clarify some aspects of these issues.

With regard to possible solutions for the protection of lithoid materials against weathering, the field of nanolime and nanosilica coatings has recently been developing for the consolidation of lime-based stones/plaster/mortars and siliceous stones, respectively.

These products are very inexpensive compared with inorganic and organic products (such as ethyl silicate and acrylic and silicone resins) that have been traditionally used for the past fifty years, but are in the process of being technologically surpassed.

As far as the rise of the sea level is concerned, we point out how meteorological and astronomical tides can contribute to a further rise in sea level. Simulation software can be used to better understand the effect of waves.

Although projections are made for the year 2100 A.D., coastal erosion problems especially are ongoing within the Nora archaeological area. It is therefore evident that extraordinary maintenance interventions must be performed in the coming years. These range from the consolidation of stone materials to the reinforcement of rocky ridges against coastal erosion. If the area were flooded, the behavior of the stone materials would depend on their physical–mechanical characteristics. Some materials have already exhibited decohesion when submerged during the total absorption test at atmospheric pressure (Table 1). Although the test was performed in standing water, sea currents and waves could damage the material further. The physical–chemical reaction of submerged stone in seawater is rather uncertain. Algal colonization that is very common in the Mediterranean sea (*chlorophyta, rhodophyta*) could create a protective layer which is commonly called "noble patina". A simultaneous acidification of the pH of seawater, a phenomenon that is constantly progressing, could contribute to an increasingly rapid dissolution of the carbonate matrix of sandstones.

Funding: This work was funded by the Recursos Humanos Altamente Qualificados (University of Evora) with program Reference: ALT2059-2019-24.

Institutional Review Board Statement: Not applicable.

Informed Consent Statement: Not applicable.

Data Availability Statement: Not applicable.

Conflicts of Interest: The author declares no known competing financial interests or personal relationships that could have appeared to influence the work reported in this paper.

References

1. Fabio, S.; Massimo, B.; Stefano, C.; Carla, L.; Catarina, M.; José, M. Ancient Restoration and Production Technologies of Roman Mortars from Monuments Placed in Hydrogeological Risk Areas: A Case Study. *Archaeol. Anthropol. Sci.* **2020**, *12*, 147. [CrossRef]
2. Reimann, L.; Vafeidis, A.T.; Brown, S.; Hinkel, J.; Tol, R.S.J. Mediterranean UNESCO World Heritage at Risk from Coastal Flooding and Erosion Due to Sea-Level Rise. *Nat. Commun.* **2018**, *9*, 4161. [CrossRef]
3. Sitzia, F.; Lisci, C.; Mirão, J. The Interaction between Rainwater and Polished Building Stones for Flooring and Cladding—Implications in Architecture. *J. Build. Eng.* **2022**, *52*, 104495. [CrossRef]
4. Spiker, E.C.; Hosker, R.P.; Weintraub, V.C.; Sherwood, S.I. Laboratory Study of SO2 Dry Deposition on Limestone and Marble: Effects of Humidity and Surface Variables. *Water Air Soil Pollut.* **1995**, *85*, 2679–2685. [CrossRef]
5. Sitzia, F.; Peters, M.J.H.; Lisci, C. Climate Change and Its Outcome on the Archaeological Areas and Their Building Materials. The Case Study of Tharros (Italy). *Digit. Appl. Archaeol. Cult. Herit.* **2022**, *25*, 1–17. [CrossRef]
6. Vousdoukas, M.I.; Clarke, J.; Ranasinghe, R.; Reimann, L.; Khalaf, N.; Duong, T.M.; Ouweneel, B.; Sabour, S.; Iles, C.E.; Trisos, C.H.; et al. African Heritage Sites Threatened as Sea-Level Rise Accelerates. *Nat. Clim. Chang.* **2022**, *12*, 256–262. [CrossRef]
7. Pesce, G. *Nora, Guida Agli Scavi*; Cagliari, Italy, 1972. Available online: https://www.amazon.it/Nora-Guida-agli-scavi-Genanro-Pesce/dp/B009A90X2C (accessed on 15 July 2022).
8. Tronchetti, C. *Nora*; Sassari, Italy, 2001. Available online: http://nora.beniculturali.unipd.it/storia-del-sito/bibliografia-essenziale/ (accessed on 15 July 2021).
9. Zucca, R. *Tharros*; Oristano, Italy, 1993. Available online: https://iris.uniss.it/bitstream/11388/262836/1/Zucca_R_Codex_multiplex_da_Tharros.pdf (accessed on 15 July 2021).
10. Macnamara, E. Underwater Exploration of the Ancient Port of Nora, Sardinia. *Pap. Br. Sch. Rome* **1967**, *35*, 4–11. [CrossRef]

11. Di Gregorio, F.; Floris, C.; Matta, P. Ricerche Su Nora I (Anni 1990–1998). In *Ricerche Su Nora I (Anni 1990–1998)*; Soprintendenza Archeologica per le Province di Cagliari e Oristano: Cagliari, Italy, 2000; pp. 9–18.
12. Bonetto, J.; Falezza, G.; Bertelli, A.; Ebner, D. Nora e Il Mare. Il Progetto Noramar. Attività 2011. In *Quaderni Norensi*; Padova University Press: Padova, Italy, 2012; pp. 327–338.
13. Bonetto, J.; Zara, A. The Nora Virtual Tour: An Immersive Visit in the Ancient City. *Archeol. e Calc.* **2017**, *28*, 531–538.
14. Carraro, F.; Marinello, A.; Morabito, D.; Bonetto, J. New Perspectives on the Sanctuary of Aesculapius in Nora (Sardinia): From Photogrammetry to Visualizing and Querying Tools. *Open Archaeol.* **2019**, *5*, 263–273. [CrossRef]
15. Agapiou, A.; Lysandrou, V.; Hadjimitsis, D.G. Earth Observation Contribution to Cultural Heritage Disaster Risk Management: Case Study of Eastern Mediterranean Open Air Archaeological Monuments and Sites. *Remote Sens.* **2020**, *12*, 1330. [CrossRef]
16. Zaina, F.; Cuca, B. Damages to Archaeological Heritage Recorded, Documented and Monitored Using Geospatial Technologies: An Assessement of Indexed Literature. In Proceedings of the IEEE, Mediterranean and Middle-East Geosciences and Remote Sensing Symposium, Istanbul, Turkey, 7–9 March 2022; pp. 110–113.
17. Deiana, G.; Antonioli, F.; Moretti, L.; Orrù, P.E.; Randazzo, G.; Lo Presti, V. MIS 5.5 Highstand and Future Sea Level Flooding at 2100 and 2300 in Tectonically Stable Areas of Central Mediterranean Sea: Sardinia and the Pontina Plain (Southern Latium), Italy. *Water* **2021**, *13*, 2597. [CrossRef]
18. Sitzia, F.; Lisci, C.; Mirão, J. Accelerate Ageing on Building Stone Materials by Simulating Daily, Seasonal Thermo-Hygrometric Conditions and Solar Radiation of Csa Mediterranean Climate. *Constr. Build. Mater.* **2020**, *266*, 121009. [CrossRef]
19. Sitzia, F.; Lisci, C.; Mirão, J. Building Pathology and Environment: Weathering and Decay of Stone Construction Materials Subjected to a Csa Mediterranean Climate Laboratory Simulation. *Constr. Build. Mater.* **2021**, *300*, 124311. [CrossRef]
20. Massidda, L.; Sanna, U. La Cristallizzazione Salina Nei Materiali Da Costruzione. *Enco J.* **2001**, *14*, 8–9.
21. Massidda, L.; Atzeni, C.; Sanna, U. Acquisizione Di Dati Su Processi Di Degrado e Interventi Di Consolidamento Alle Terme a Mare Di Nora (Pula, CA). Relazione Finale Della Convenzione/Contratto Del 18-07-1994 Stipulata Con La Soprintendenza Archeologica per Le Provincie Di Cagliari Ed Orist. 1994. Available online: https://nora.beniculturali.unipd.it/wp-content/uploads/2015/06/7_Ricerche_su_Nora_1.pdf (accessed on 15 July 2021).
22. Assorgia, A.; Barca, S.; Spano, C. Lineamenti Stratigrafici, Tettonici e Magmatici Del Teziario Della Sardegna. In Proceedings of the Convegno Sulla Fossa Sarda; Villanovaforru, Italy, 19–22 June 1997; pp. 13–25.
23. Beccaluva, L.; Leone, F.; Civetta, L.; Macciotta, G.P.; Ricci, C.A. Geochronology in Sardinia: Results and Problems. *Rend. Della Soc. Ital. Di Mineral. E Petrogr.* **1985**, *40*, 57–72.
24. Carmignani, L.; Oggiano, G.; Funedda, A.; Conti, P.; Pasci, S. The Geological Map of Sardinia (Italy) at 1:250,000 Scale. *J. Maps* **2015**, *12*, 826–835. [CrossRef]
25. Biste, M. Geochemistry of South Sardinian Granites Compared with Their Tin Potential. *Met. Assoc. Acid Magmat.* **1982**, *37*, 49.
26. Zara, A. *Evoluzione Urbana e Nuovo Assetto Monumentale Di Nora in Età Medio-Imperiale Romana*; University of Padova: Padua, Italy, 2011.
27. Columbu, S.; Gioncada, A.; Lezzerini, M.; Sitzia, F. Mineralogical-Chemical Alteration and Origin of Ignimbritic Stones Used in the Old Cathedral of Nostra Signora Di Castro (Sardinia, Italy). *Stud. Conserv.* **2019**, *64*, 397–422. [CrossRef]
28. Columbu, S. Petrographic and Geochemical Investigations on the Volcanic Rocks Used in the Punic-Roman Archaeological Site of Nora (Sardinia, Italy). *Environ. Earth Sci.* **2018**, *77*, 577. [CrossRef]
29. Garau, A.M. *Le Pietre e Le Malte Del Teatro Di Nora (Sardegna SW)*; Università degli studi di Cagliari: Cagliari, Italy, 2005.
30. Finocchi, S. Nora e Il Territorio: Le Risorse Minerarie. In *Proceedings of the Nora area C. Scavi 1996–1999;* Giannattasio, B.M., Ed.; Genova, Italy, 2003; pp. 31–33.
31. Previato, C. *Nora. Le Cave Di Pietra Della Città Antica*; Quasar: Rome, Italy, 2016.
32. Fadda, A.F. *Sardegna, Guida Ai Tesori Nascosti*; Coedisar: Cagliari, Italy, 1994.
33. Billows, E. *Lessico Mineralogico per l'Isola Di Sardegna*; Ledda: Cagliari, Italy, 1922.
34. Bechstädt, T.; Boni, M.; Schledding, T. Slope-Sediments in the Cambrian Gonnesa Formation of the Sulcis Area, SW-Sardinia. *Neues Jahrb. Für Geol. Und Paläontologie—Mon.* **1984**, *1984*, 129–138. [CrossRef]
35. Vannelli, V. *Guida Al Verde Di Teulada e Del Suo Territorio*; Cuec: Cagliari, Italy, 2001.
36. Palmström, A. RMi-A for Rock Mass Characterization System for Rock Engineering Purposes. Ph.D. Thesis, The University of Oslo, Oslo, Norway, 1995.
37. Masson-Delmotte, V.; Zhai, P.; Pirani, A.; Connors, S.L.; Péan, C.; Berger, S.; Caud, N.; Chen, Y.; Goldfarb, L.; Gomis, M.I.; et al. IPCC,2021: Climate Change 2021: The Physical Science Basis. In *Contribution of Working Group I to the Sixth Assessment Report of the Intergovernmental Panel on Climate Change*; 2021.
38. Peltier, L.C. The Geographic Cycle in Periglacial Regions as It Is Related to Climatic Geomorphology. *Ann. Assoc. Am. Geogr.* **1950**, *40*, 214–236. [CrossRef]
39. Sequeira Braga, M.A.; Paquet, H.; Begonha, A. Weathering of Granites in a Temperate Climate (NW Portugal): Granitic Saprolites and Arenization. *Catena* **2002**, *49*, 41–56. [CrossRef]
40. Sitzia, F.; Beltrame, M.; Lisci, C.; Mirao, J. Micro Destructive Analysis for the Characterization of Ancient Mortars: A Case Study from the Little Roman Bath of Nora (Sardinia, Italy). *Heritage* **2021**, *4*, 2544–2562. [CrossRef]
41. Mustoe, G.E. The Origin of Honeycomb Weathering. *Geol. Soc. Am. Bull.* **1982**, *93*, 108. [CrossRef]
42. Mottershead, D.N.; Pye, K. Tafoni on Coastal Slopes, South Devon, U.K. *Earth Surf. Process. Landf.* **1994**, *19*, 543–563. [CrossRef]

43. Riahi, K.; van Vuuren, D.P.; Kriegler, E.; Edmonds, J.; O'Neill, B.C.; Fujimori, S.; Bauer, N.; Calvin, K.; Dellink, R.; Fricko, O.; et al. The Shared Socioeconomic Pathways and Their Energy, Land Use, and Greenhouse Gas Emissions Implications: An Overview. *Glob. Environ. Chang.* **2017**, *42*, 153–168. [CrossRef]
44. Rogelj, J.; Popp, A.; Calvin, K.V.; Luderer, G.; Emmerling, J.; Gernaat, D.; Fujimori, S.; Strefler, J.; Hasegawa, T.; Marangoni, G.; et al. Scenarios towards Limiting Global Mean Temperature Increase below 1.5 °C. *Nat. Clim. Chang.* **2018**, *8*, 325–332. [CrossRef]
45. Bonazza, A.; Messina, P.; Sabbioni, C.; Grossi, C.M.; Brimblecombe, P. Mapping the Impact of Climate Change on Surface Recession of Carbonate Buildings in Europe. *Sci. Total Environ.* **2009**, *407*, 2039–2050. [CrossRef]
46. Lipfert, F.W. Atmospheric Damage to Calcareous Stones: Comparison and Reconciliation of Recent Experimental Findings. *Atmos. Environ.* **1989**, *23*, 415–429. [CrossRef]
47. Rodhe, H.; Dentener, F.; Schulz, M. The Global Distribution of Acidifying Wet Deposition. *Environ. Sci. Technol.* **2002**, *36*, 4382–4388. [CrossRef]
48. *Prentice The Carbon Cycle and Atmospheric Carbon Dioxide*; Cambridge University Press: Cambridge, UK, 2001.
49. Gregorio, F.D.; Pusceddu, M.; Romoli, E.; Serreli, A.; Carlo, T.; Ambientale, G. Valutazione Del Rischio d' Erosione Costiera Nell' Area Archeologica Di Nora (Sardegna SW). In Proceedings of the Atti 14a Conferenza Nazionale ASITA, Brescia, Italy, 9–12 November 2010; pp. 869–874.
50. Di Gregorio, F.; Floris, C.; Matta, P.; Roppa, A. *Il Quadro Am- Bientale, in Nora. Il Foro Romano. Storia Di UN'AREA Urbana DALL'ETÀ Fenicia Alla Tarda Antichità*; Italgraf (Noventa Padovana): Padova, Italy, 2009.
51. Lambeck, K.; Purcell, A. Sea-Level Change in the Mediterranean Sea since the LGM: Model Predictions for Tectonically Stable Areas. *Quat. Sci. Rev.* **2005**, *24*, 1969–1988. [CrossRef]